Dye-Sensitized Solar Cells Based on Anatase TiO_2 Nanoparticle/Nanowire Composites

Bing Tan and Yiying Wu*

Department of Chemistry, The Ohio State University, Columbus, Ohio 43210

Received: June 25, 2006; In Final Form: June 28, 2006

Dye-sensitized solar cells were fabricated based on the composites of anatase TiO_2 nanoparticles and single crystalline anatase TiO_2 nanowires. Nanoparticle/nanowire composites can possess the advantages of both building blocks, i.e., the high surface area of nanoparticle aggregates and the rapid electron transport rate and the light scattering effect of single-crystalline nanowires. Three different composites were prepared with 5 wt %, 20 wt %, and 77 wt % nanowires, respectively. The performances of composite solar cells were compared with pure nanoparticle cells at a series of film thickness. With low nanowire concentrations (5 wt % and 20 wt %), the composite films maintain similar specific surface area as the pure nanoparticle films, while the composite cells show higher short-circuit current density and open-circuit voltage. An enhancement of power efficiency from 6.7% for pure nanoparticle cells to 8.6% for the composite cell with 20 wt % nanowires has been achieved under 1 Sun AM1.5 illumination (100 mW/cm^2). For the composite film with 77 wt % nanowires, the nanowires became the major phase. Their less compact packing resulted in significant decrease of the specific surface area, and thus the current density. However, with the increase of film thickness, the current density showed a continuous increase in the whole thickness range up to 17 μm, indicating the improved electron diffusion length due to the formed nanowire network. The nanowires also helped to preserve crack-free thick films. These results show that employing nanoparticle/nanowire composites represents a promising approach for further improving the efficiencies of sensitized solar cells.

1. Introduction

Since the breakthrough work by Grätzel in 1991, dye-sensitized solar cells (DSSCs) based on TiO_2 nanoparticles have attracted extensive attentions from both industry and academia.[1,2] Compared to the conventional silicon p−n junction cells in market, DSSCs hold the promise of lower fabrication cost and have efficiencies comparable to amorphous silicon solar cells. The main components in these DSSCs are a high-surface-area TiO_2 film on a transparent conducting glass, the adsorbed dye sensitizers, and an electrolyte solution penetrating throughout the TiO_2 film. In the operation, the sunlight is absorbed by the dye molecules and excites electrons from HOMO to LUMO, which then inject into the TiO_2 electrode. These electrons percolate through the TiO_2 film and are collected by the conducting substrate. The oxidized dye molecules are regenerated by the reducing species in the electrolyte solution, predominately I^- ions. The overall light-to-electricity efficiency is affected by many factors, including the Pt catalyst,[3] the transmittance and the conductivity of the conducting substrate,[4,5] the electrolyte composition,[6] type of dye sensitizer,[7] and properties of TiO_2 film.[8,9]

The rapid electron transport in the TiO_2 film is important to ensure their efficient collection by the conducting substrate when in competition with the recombination processes. The electrons transport through a slow trap-limited diffusion process.[10] In an anatase TiO_2 nanoparticle film, the electron diffusion coefficient is more than 2 orders of magnitude lower than in single crystals.[11] In the diffusion process, electrons may recombine with the oxidizing species, predominately triiodide ions in the electrolyte. Electron diffusion lengths of 7−30 μm have been reported for cells operating at light intensities up to 0.1 Sun,[12−14] which impose an upper limit of the TiO_2 film thickness, and thus the roughness factor and light harvesting.

Fabrication of films from one-dimensional nano-structures has proven to be an effective way to facilitate electron transport.[15−28] Law et al. found the electron diffusion coefficient of ZnO nanowires is several hundred times larger than the coefficient for ZnO or TiO_2 nanoparticle film.[23] Ohsaki et al. reported that the electron life of a nanotube film is improved by 3 times greater than that in a nanoparticle film resulting in an improvement of diffusion length.[24] A consistent observation is later reported by Mor et al. [28] The authors measured that the nanotube films have superior electron life than nanoparticle films.[28]

In addition to the effect on electron transport, nanowires can also scatter light and thus enhance the light harvesting. In most conventional DSSCs, TiO_2 nanoparicles with sizes of 15−20 nm were used. The sizes are much smaller than the wavelength of visible light. The film is thus transparent with little light scattering. Incorporation of large nanoparticles (100 nm − 400 nm) has been employed as light-scattering centers to increase the optical length in the film, and an enhanced light-harvesting has been demonstrated both experimentally[9,29] and theoretically.[30−32] Incorporation of nanowires with lengths in the range of hundreds of nanometers to several micrometers should have similar effect.

Therefore, the nanoparticle/nanowire composites can represent a very versatile structure. The nanoparticles can provide large surface areas for the dye adsorption, while the incorporated nanowires can enhance the light harvesting, electron transport rate, and also the mechanical properties of the films. So far, there have been limited investigations on this system. For example, with the mixture of 5 wt % TiO_2 nanowires in nanoparticles, Sanehira et al. improved the overall efficiency from 5.84% to 6.24%.[19] No information about the crystal structure of the TiO_2

* Corresponding author e-mail: wu@chemistry.ohio-state.edu.

10.1021/jp063972n CCC: $33.50
Published on Web 07/25/2006

nanowires was given out by the authors and there was only one composition studied. Recently, Yoon et al. reported the incorporation of TiO_2 nanorods into a P25 nanoparticle film.[33] With an increase of the amount of nanorods, the short-circuit current increased, but the fill factor decreased. Besides TiO_2, infiltration of ZnO nanoparticle into vertically aligned ZnO nanowires has been reported by Baxter et al.[34] An improvement in the overall light to electricity efficiency from 0.5% to 1.1% has been obtained.

In this report, we used the composites of anatase TiO_2 nanoparticles and single-crystalline anatase TiO_2 nanowires as electrodes to fabricate DSSCs, and systematically investigated the effect of the relative nanowire/nanoparticle ratio on the performance of solar cells. When the nanowires are less than 20 wt % in the composite films, the internal surface area of the composite was measured to be similar to that of a pure nanoparticle film. With 5 wt % and 20 wt % nanowires, the composite cells showed higher short-circuit current density than pure nanoparticle cells. In our studies, the best overall light-to-electricity efficiency was 6.7% for pure nanoparticle cells under 1 Sun AM1.5 simulated sunlight. By adding 20 wt % nanowires the efficiency had reached 8.6%. In addition, incorporating nanowires in nanoparticles also facilitated the fabrication of crack-free thick films (>10 μm thick) from one deposition. These results showed that by carefully controlling the concentration of nanowires, nanoparticle/nanowire composites can possess the advantages of both building blocks, i.e., the high surface area of nanoparticle aggregates and the long electron diffusion length and light scattering effect of single-crystalline nanowires, and thus represent a promising approach for further improving the efficiencies of sensitized solar cells.

2. Experimental Methods

2.1. Preparation of TiO_2 Nanoparticles and Nanowires. TiO_2 nanoparticles with size around 18 nm were prepared according to the reported procedure.[35] XRD pattern confirms the nanoparticles have pure anatase structure (Supporting Information Figure S1). TiO_2 nanowires with pure anatase phase were prepared from a modified hydrothermal process.[36] Six grams of TiO_2 nanopowder (99.9%, average size: 25−70 nm, Aldrich) was mixed with 33 mL NaOH (15 M) aqueous solution with stirring at room temperature for 10 min. The mixture was then heated at 170 °C for 3 days in a 125 mL Teflon-lined autoclave. The collected precipitates were washed with dilute HCl and water for several times. The final product was obtained by calcining the washed precipitates at 700 °C for 2 h. No sodium impurity was observed in the final product from energy-dispersive X-ray spectra (EDS).

2.2. Fabrication of DSSC Cells. Four pastes containing mixed TiO_2 nanoparticles and nanowires (labeled as P1W0, P9.5W0.5, P8W2, and P2.3W7.7) were prepared with nanowires concentration of 0, 5, 20, and 77 wt %, respectively. P1W0, therefore, represents the pure nanoparticle sample. A paste was prepared by first ultrasonically mixing nanoparticles (~5 wt % from the hydrothermal process) and nanowires (22 wt % in 0.1 M aqueous HNO_3) solutions for 1 h. The mixed solution was then added with polyethylene glycol (PEG, molecular weight: 20 000, Alfa Aesar). The solution was then concentrated by heating to obtain a viscous paste. The quality of the prepared nanoparticles was reported to influence the performance of the cells.[37] To avoid the difference from the nanoparticle quality, all pastes were prepared from the same batch of nanoparticles.

The TiO_2 composite films were prepared by the doctor blade technique. The edges of a conducting glass (TEC-8, Hartford Glass Co, IN) were covered with adhesive tapes as the frame. Paste was flattened with a glass rod. Films with different thickness were fabricated by adjusting the concentration of the paste and the layer numbers of the tape. For pure nanoparticle films, the fabricated thick films (>10 μm) from one-deposition tended to have cracks after sintering caused by a contraction of volume.[38] The active materials of porous TiO_2 are missing within the cracks. This will reduce the internal surface area, leading to a reduced dye adsorption and thus a reduced short-circuit current. Only those with good dye adsorption were discussed in this report. After calcined at 450 °C for 30 min, films were treated with 0.2 M $TiCl_4$ for 13 h.[7] The treated films were then calcined at 450 °C for another 30 min before cooling down to 100 °C for dye sensitization.

The dye solution was prepared by dissolving 0.17 mM cis-di(thiocyanato)bis(2,2′-bipyridyl-4,4′-dicarboxylate)rutheniium-(II) (also called N719, Solaronix SA, Switzerland) in dry ethanol. Dye sensitization was accomplished by immersing a TiO_2 film in dye solution for at least 36 h in a sealed beaker. The extent of sensitization was estimated by comparing the colors at the top and the bottom of the film. The sensitization was completed after the colors at the top and the bottom were the same. The film was left in dye solution at least for another 12 h to reduce the possibility of incomplete sensitization. Films made from P1W0 and P2.3W7.7 were sensitized over 36 h. Thin films (<10 μm) from P9.5W0.5 and P8W2 were sensitized for 36 h, while thick films (≥ 10 μm) were stayed in dye solution for 6 days (10~15 μm) or 12 days (>15 μm). Since dyes are monolayered adsorbed, extra sensitization time is not expected to affect the amount of dyes adsorbed under the careful protection from exposing to moisture. To confirm the expectation, a film from P1W0 with 11.5 μm thickness was sensitized with different times. Dye loadings were the same when the film was sensitized for 1 day or 7 days.

A solar cell was assembled by placing a platinum-coated conducting glass on the dye-sensitized electrode separated by a 60 μm polymer spacer (Solaronix SA, Switzerland). The assembled cell was then clipped together as an open cell. An electrolyte was made with 0.1 M LiI (Aldrich), 0.1 M I_2 (Aldrich), 0.6 M tetrabutylammonium iodide (Fluka), and 0.5 M *tert*-butylpyridine (Aldrich) in dry acetonitrile (Fluka). To ensure the same batch of electrolyte was used for every sample, a larger amount of electrolyte solution was prepared at first and then divided into several smaller glass vials. All vials were sealed and stored in a vacuum desiccator. The electrolyte was injected into the open cell from the edges, and the cell was tested immediately. After testing, the dye from a film was desorbed in a 0.1 M NaOH aqueous solution to measure the roughness factor (defined as the total surface area per unit substrate area) after removing the electrolyte with ethanol. A value of 1.6 nm^2/dye molecule [39] was used to estimate the roughness factor.

2.3. Characterization and Measurements. TiO_2 nanoparticles and nanowires were characterized with Rigaku X-ray powder diffractometer, Sirion scanning electron microscope (SEM), and Tecnai TF-20 transmission electron microscopy (TEM). Optical images were taken with a digital camera (Canon PowerShot S400). Film thickness was measured with a computerized profilometer (Dektak 3). The amount of dye adsorbed was measured with UV−vis spectroscopy. UV−vis absorption and transmission spectra were recorded with a Lambda 6, UV−Vis spectrometer (Perkin-Elmer, UK). A blank conducting glass was used as the reference sample. A film was illuminated from the conducting glass side. Reflection spectra were collected in air using lambda 19, UV−Vis spectrometer (Perkin-Elmer, UK)

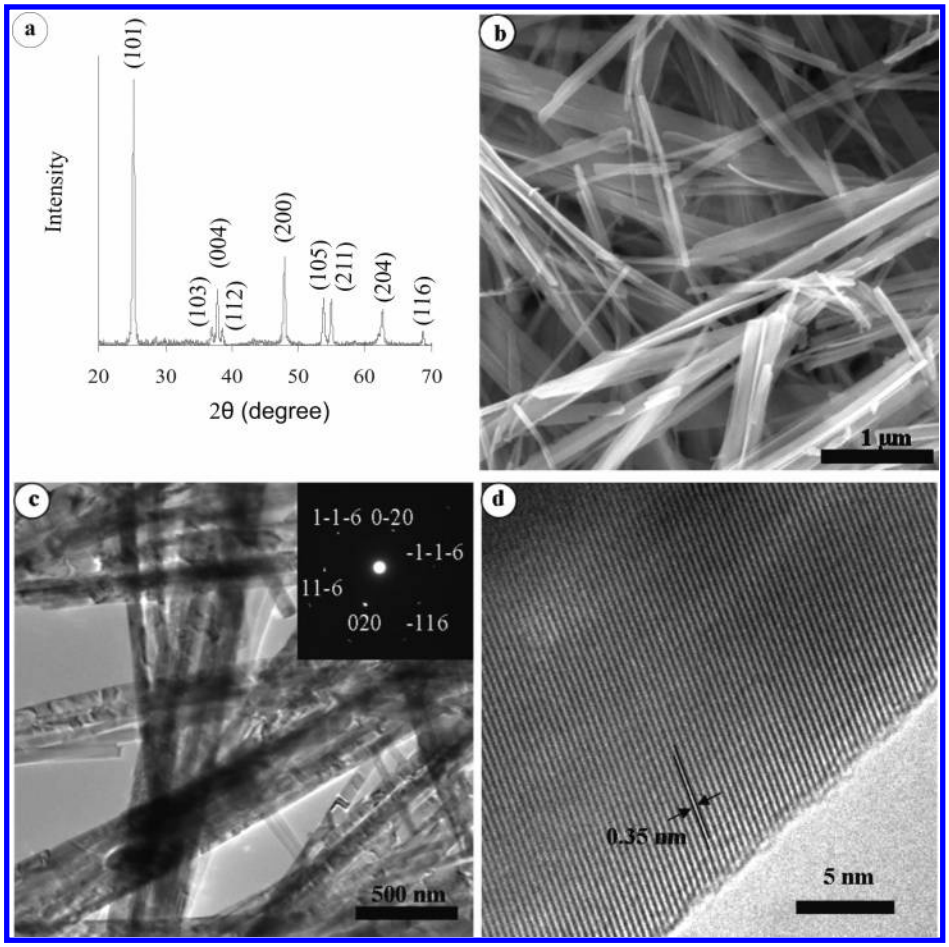

Figure 1. Characterizations of the TiO_2 nanowires: (a). XRD pattern; (b) SEM image of nanowires; (c) TEM image of nanowires (inset: SAED of a single nanowire indexed along [601] zone axis); (d) High-resolution TEM image of a nanowire. The spacing between adjacent layers was 0.35 nm, corresponding to the distance between (1 0 1) planes in an anatase structure.

connected to an intergrating sphere accessory. The incident beam was at 8 degrees close to a normal incident. The reflection spectrum of a blank conducting glass was collected for comparison. For all samples, the glass side away from the light source was coated with dark paint to avoid any reflection from the background. Photovoltaic characterization was performed under 1 Sun AM 1.5 G simulated sunlight (Small-Area Class-B solar simulator, PV Measurements). There is a slight mismatch between the simulated and the reference AM 1.5 G sunlight (Supporting Information Figure S2). The light from our simulator has a higher irradiance between 500 and 660 nm than the AM 1.5 global reference spectrum with a peak centered at ~580 nm, which corresponds to one of the absorption bands of the dye N-719 (Supporting Information Figure S3). This caused a slight increase of current density compared to the cell performance under standard AM 1.5 reference illumination.[40] The mismatch, however, will not affect our comparison among films made from pure nanoparticles and nanoparticle/nanowire composites, and therefore, the systematic trends. I−V curves were recorded with a CV-50W voltammetric analyzer. A black-painted mask was used to create an exposed area of 0.20 cm^2 for all samples.

3. Results and Discussion

3.1. Preparation and Characterization of TiO_2 Single-Crystalline Nanowires. XRD pattern shows that the nanowires after being calcined at 700 °C were pure anatase phase (Figure 1a). TEM (Figure 1c) images showed that the nanowires have diameters in the range of 30−80 nm, and tend to form bundles as shown in SEM (Figure 1b) images. The nanowires had length from hundreds nanometers to several micrometers. The single-crystallinity of the nanowires was confirmed by the selected area electron diffraction pattern (SAED, inset in Figure 1c) and high-resolution TEM (Figure 1d).

3.2. Solar Cells Based on Monolayer Nanoparticle/Nanowire Composites. Cross-section SEM images of films made from P1W0, P9.5W0.5, P8W2, and P2.3W7.7 pastes are shown in Figure 2. Films from P1W0, P9.5W0.5, and P8W2 were compact (Figure 2a−c). Besides the void spaces between individual nanoparticles, there are few large void spaces. Small bundles of thin nanowires were embedded in nanoparticles for P9.5W0.5 and P8W2 samples. Cross-section of P2.3W7.7 film (Figure 2d), on the other hand, showed less compact structure with large void spaces of several hundred nm in size due to the high concentration of nanowires. An example is indicated by the arrow in Figure 2d. As shown below, this will cause a significant decrease of specific surface area.

The optical images of the films before and after dye adsorption are displayed in Figure 3. All films had the same thickness of 10 μm. To visually compare the transparency, a piece of white paper written with "OHIO" was used as the background. Before dye adsorption, the pure nanoparticle film was only slightly opaque. The letter "O" can be clearly observed. With the addition of 5 wt % of nanowires, the film became opaque, but the letter "H" can still be observed. With the addition of 20 wt % of nanowires, no letters from the background can be

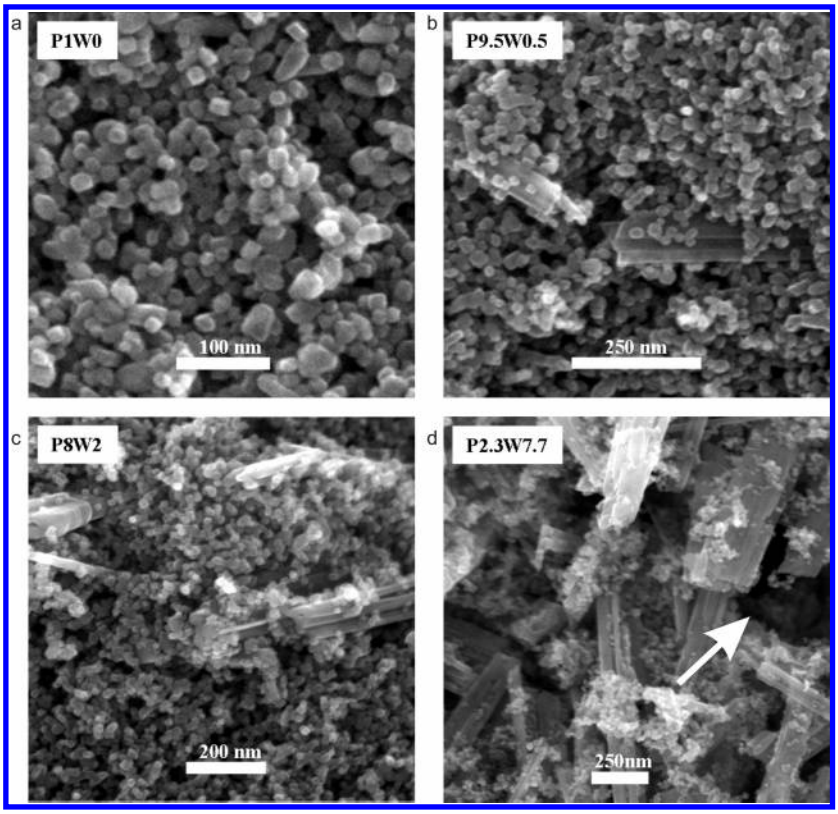

Figure 2. Cross-section SEM images for films made from (a) P1W0, (b) P9.5W0.5, (c) P8W2, and (d) P2.3W7.7 pastes. The arrow in (d) indicates an example of the large void space between nanowires.

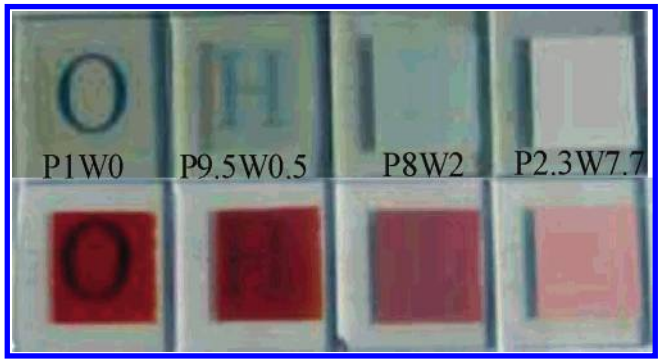

Figure 3. Optical images of the films before and after dye adsorption taken by a digital camera.

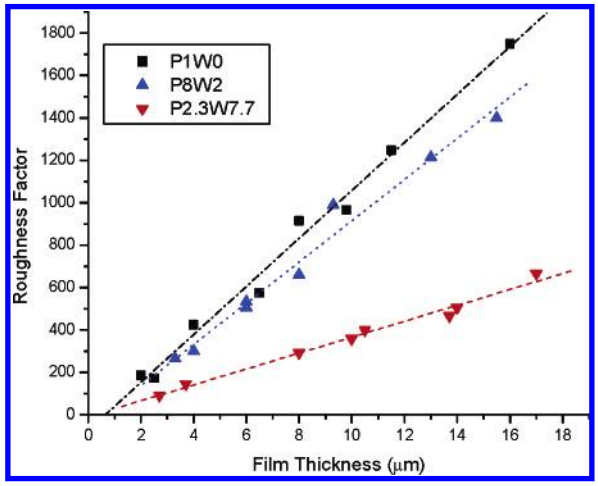

Figure 4. Dependence of roughness factor on film thickness. The roughness factor data of P9.5W0.5 sit between P1W0 and P8W2. Data not shown for the clarity of graph.

observed. With 77 wt % of nanowires, the film became completely white. Therefore, with an increase of nanowires, the film became more and more opaque due to the light scattering effect by embedded nanowires. A trend similar to this was observed on the transmission and reflection spectra of these films (see Supporting Information Figure S4) Films after dye adsorption are also displayed in Figure 3. Both films made from P1W0 and P9.5W0.5 had dark red colors, while the film made from P2.3W7.7 had a pink color. The color of the film made from P8W2 was between dark red and pink. The background letters can be identified for films made from P1W0 and P9.5W0.5, but not for P8W2 and P2.3P7.7.

The roughness factors of these films, calculated based on the amount of adsorbed dye molecules, are shown in Figure 4. For all films with a fixed composition, there was a linear relationship between the film thickness and the roughness factor. This suggests that all films had been completely sensitized, otherwise a deviation from the linear relationship should be observed. There was only a slightly decrease (by <14%) in the dye adsorption with the increase of nanowires up to 20 wt %, while the dye adsorption was much lower when the nanowires increased to 77 wt % (decrease by 67%). Considering the cross-section SEM images of these films shown in Figure 2, we suggest that when the nanowire concentration is low (<20 wt %), the individual nanowires (or bundles) are still far from each other, and therefore, do not perturb the compact packing of the nanocrystals. When the nanowire concentration is high (e.g., 77 wt % in this study), the nanowires and their bundles become the major phase. Their assembly forms less compact packing with large empty spaces as shown in Figure 2d. This caused a significant decrease of specific surface area of the P2.3W7.7 films. The smaller specific surface area of nanowires than nanoparticles should also contribute to the decrease of roughness factor.

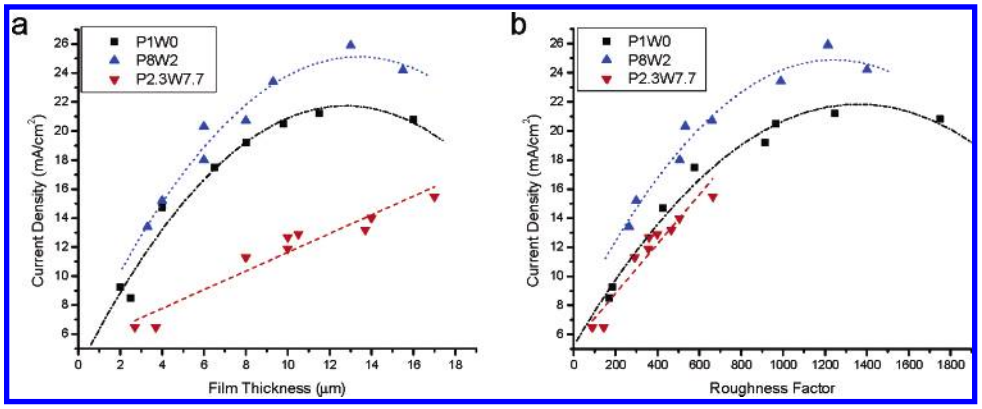

Figure 5. Dependence of short-circuit current on: (a), film thickness; (b), roughness factor. The data of P9.5W0.5 overlap with P8W2. They are not shown here for the clarity of graph. Same for Figures 6 and 7.

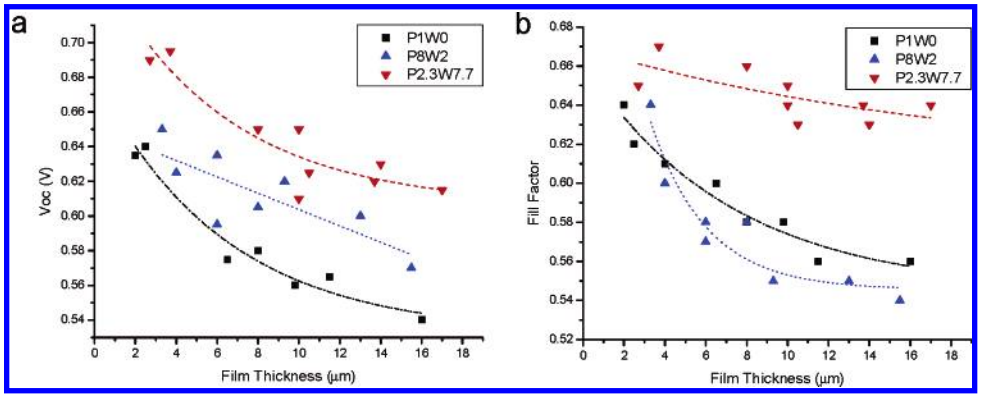

Figure 6. Dependence of (a) open-circuit voltage and (b) fill factor on film thickness.

The performances of the DSSCs based on these films were then measured under 1 Sun AM 1.5 simulated sunlight. The short-circuit current density profiles plotted vs film thickness and roughness factor are displayed in Figures 5a and b, respectively. The current densities had a similar trend with an increase of film thickness for P1W0, P9.5W0.5, and P8W2 films: they first increase with the thickness, then flatten out when the thickness is beyond 10 μm with a slight decline. P9.5W0.5 and P8W2 cells are saturated slightly slower than pure nanoparticle films with higher current densities. On the contrary, P2.3W7.7 cells with much higher nanowire concentrations show significantly lower current densities, but the current densities increase continuously with the film thickness in the whole range up to 17 μm.

As discussed earlier, the incorporation of nanowires into nanoparticle films affects the specific surface area, light scattering, electron transport rate, and also the porosity. The relative importance of these effects depends on the nanowire concentration. The P9.5W0.5 and P8W2 films have slightly lower surface areas as the P1W0 films (Figure 4). Therefore, the higher current density from P9.5W0.5 and P8W2 films should not come from dye loading. The possible reasons include light scattering by the nanowires and the increased rate of electron transport through nanowires. For these films with dilute nanowire concentration, there is no connected nanowire network for electrons to transport (Figure 2), and therefore, the rate-limiting step of electron transport should still be the diffusion process through the nanoparticle aggregates. The current densities of these films also show a similar trend, with an increase of film thickness as P1W0 films. Therefore, we speculate the light scattering effect is the major reason for the enhanced current density of P9.5W0.5 and P1W0 cells. On the other hand, the P2.3W7.7 films have significantly lower surface area. High concentration of nanowires can also scatter light out of cells. Both effects decrease light harvesting and thus cause lower current density. However, nanowires become the major phase in these films, and thus they can form networks for the electron transport. This explains the continuous increase of the current density with the film thickness. Phenomena similar to this have been observed for cells made from oriented-attached nanoparticles.[17]

Open-circuit voltages (V_{oc}) of the films are compared in Figure 6a. For all films, the V_{oc} values decreased with an increase of the film thickness. The decrease was explained as a consequence of increased charge recombination and restricted mass transport in thicker films.[9] With the same film thickness, the V_{oc} from P2.3W7.7 was higher than that from P1W0, P9.5W0.5, or P8W2. Generally, the V_{oc} of a pure nanoparticle film was slightly lower than that from P8W2 or P9.5W0.5. The difference between P9.5W0.5 and P8W2 was not obvious. The V_{oc} value of a DSSC is determined by the difference between Fermi level for electrons in the TiO_2 electrode and the redox potential of I^-/I_3^-. The higher V_{oc} of the composite cells can be explained as a consequence of reduced recombination, which results in an increase of electron density in TiO_2, and thus the shift of Fermi level. Enhancement of V_{oc} has also been observed for DSSCs made from TiO_2 nanotube films by Ohsaki et al. [24] They found that the electron lifetime in a nanotube film is three times longer than that in a nanoparticle film. The improvement in the electron lifetime was attributed to a reduced recombination between TiO_2 and the electrolyte.[24]

The fill factor is determined by the internal resistance of the cell. Films made from P2.3W7.7 had large void spaces. The internal resistance for these cells should be low since the ions can easily diffuse to the counter electrode, and electrons can also transport rapidly through nanowire networks, resulting in a high fill factor. Consistent with this expectation, fill factors

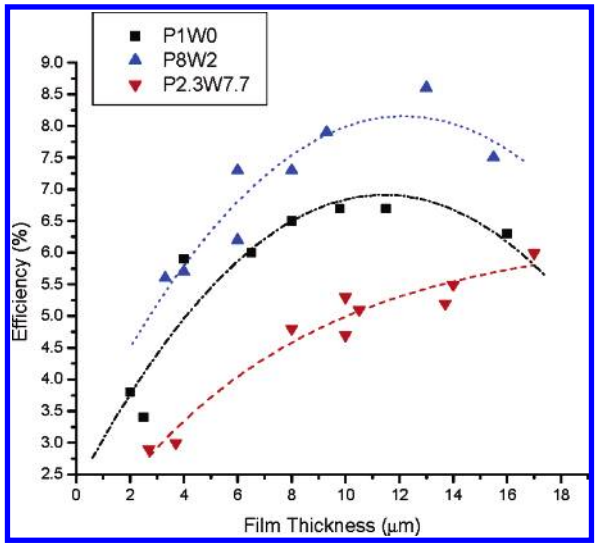

Figure 7. Dependence of overall light-to-electricity efficiency on film thickness.

from P2.3W7.7 were higher than those from other pastes (Figure 6b). The difference among P1W0, P9.5W0.5, and P8W2 was not obvious.

Putting the above parameters together, we calculated the overall power efficiency (Figure 7). Despite higher fill factors and V_{oc} values, Efficiencies of P2.3W7.7 cells were lower than the cells made form others pastes due to the low current density. The incorporation of small amount of nanowires ($\leq$20 wt %) did not change the fill factor and the V_{oc} value dramatically. The improvement in the short-circuit current would increase the overall efficiency. Efficiencies from P9.5W0.5 and P8W2 cells were higher than those from P1W0 at the film thickness from 7 to 14 μm. Among all the cells we prepared, the best efficiency was 8.6%, achieved from P8W2 cells at the film thickness of 14 μm, compared to 6.7% from our best P1W0 cells.

In addition to the effects on cell performance, the presence of nanowires also helped to preserve the crack-free films after sintering. A pure nanoparticle thick film from one deposition is easy to have cracks during sintering. This is because of the excess contraction in the film during sintering. The shrinkage of a nanowire is negligible along its long axis. The addition of small percentage of nanowires can, therefore, restrict the contraction, resulting in continuous crack-free films.

Conclusions

In summary, we used the composites of anatase TiO_2 nanoparticles and single-crystalline anatase TiO_2 nanowires as electrodes to fabricate DSSCs, and investigated the effect of the relative nanowire/nanoparticle ratio on the performance of solar cells. Encouraging improvement of solar cell efficiency has been achieved. With further optimization of the solar cell parameters including choosing dye sensitizers with a better match with the solar spectrum, the dispersion of nanowires, their concentration, and the structures of the films (e.g., multilayers), higher efficiencies might be achievable. The nanoparticle/nanowire structure will also be interesting for the fabrication of low-temperature cells on plastic substrates.[41]

Acknowledgment. The project was sponsored by start-up funding from the Ohio State University (OSU). We greatly appreciate the help from Mr. Oludurotimi Adetunji from the OSU Physics Department for reflection spectra measurements. B.T. thanks Mr. Mike Krasula from Pilkington in the U.S. for providing the conducting glass (TEC-8) at the beginning of this research.

Supporting Information Available: XRD data of the anatase TiO2 nanoparticles; Comparison between the spectrum of the solar simulator and the AM1.5 global reference spectrum; N719 dye absorption spectrum; Reflection and transmission spectra of the nanoparticle/nanowire composite films. This material is available free of charge via the Internet at http://pubs.acs.org.

References and Notes

(1) O'Regan, B.; Grätzel, M. *Nature* **1991**, *353*, 737.
(2) Grätzel, M. *Nature* **2001**, *414*, 338.
(3) Fang, X.; Ma, T.; Guan, G.; Akiyama, M.; Kida, T.; Abe, E. *J. Electroanal. Chem.* **2004**, *570*, 257.
(4) Podraza, N. J.; Chen, C.; Sainju, D.; Ezekoye, O.; Horn, M. W.; Wronski, C. R.; Collins, R. W. *Mater. Res. Soc. Symp. Proc.* **2005**, *865*(Thin-Film Compound Semiconductor Photovoltaics), 273.
(5) Lee, W. J.; Ramasamy, E.; Lee, D. Y.; Min, B. K.; Song, J. S., *Proc. SPIE-Int. Soc. Opt. Eng.* **2006**, *6038* (Photonics: Design, Technology, and Packaging II), 413.
(6) Hara, K.; Nishikawa, T.; Kurashige, M.; Kawauchi, H.; Kashima, T.; Sayama, K.; Aika, K.; Arakawa, H. *Sol. Energy Mater. Sol. Cells* **2005**, *85*, 21.
(7) Nazeeruddin, M. K.; Pechy, P.; Renouard, T.; Zakeeruddin, S. M.; Humphry-Baker, R.; Comte, P.; Liska, P.; Cevey, L.; Costa, E.; Shklover, V.; Spiccia, L.; Deacon, G. B.; Bignozzi, C. A.; Graetzel, M. *J. Am. Chem. Soc.* **2001**, *123*, 1613.
(8) Saito, Y.; Kambe, S.; Kitamura, T.; Wada, Y.; Yanagida, S. *Sol. Energy Mater. Sol. Cells* **2004**, *83*, 1.
(9) Wang, Z.-S.; Kawauchi, H.; Kashima, T.; Arakawa, H. *Coord. Chem. Rev.* **2004**, *248*, 1381.
(10) Frank, A. J.; Kopidakis, N.; van de Lagemaat, J. *Coord. Chem. Rev.* **2004**, *248*, 1165.
(11) Forro, L.; Chauvet, O.; Emin, D.; Zuppiroli, L.; Berger, H.; Lévy, F. *J. Appl. Phys.* **1994**, *75*, 663.
(12) Nakade, S.; Matsuda, M.; Kambe, S.; Saito, Y.; Kitamura, T.; Sakata, T.; Wada, Y.; Mori, H.; Yanagida, S. *J. Phys. Chem. B* **2002**, *106*, 10004.
(13) Fisher, A. C.; Peter, L. M.; Ponomarev, E. A.; Walker, A. B.; Wijayantha, K. G. U. *J. Phys. Chem. B* **2000**, *104*, 949.
(14) Oekermann, T.; Zhang, D.; Yoshida, T.; Minoura, H. *J. Phys. Chem. B* **2004**, *108*, 2227.
(15) Uchida, S.; Chiba, R.; Tomiha, M.; Masaki, N.; Shirai, M. *Electrochemistry* **2002**, *70*, 418.
(16) Uchida, S.; Chiba, R.; Tomiha, M.; Masaki, N.; Shirai, M. *Stud. Surf. Sci. Catal.* **2003**, *146*, 791.
(17) Adachi, M.; Murata, Y.; Takao, J.; Jiu, J.; Sakamoto, M.; Wang, F. *J. Am. Chem. Soc.* **2004**, *126*, 14943.
(18) Ngamsinlapasathian, S.; Sakulkhaemaruethai, S.; Pavasupree, S.; Kitiyanan, A.; Sreethawong, T.; Suzuki, Y.; Yoshikawa, S. *J. Photochem. Photobiol., A* **2004**, *164*, 145.
(19) Sanehira, Y.; Uchida, S. *Kagaku Kogyo* **2004**, *55*, 796.
(20) Baxter, J. B.; Aydil, E. S. *Appl. Phys. Lett.* **2005**, *86*, 053114/1.
(21) Guo, M.; Diao, P.; Cai, S. *Appl. Surf. Sci.* **2005**, *249*, 71.
(22) Jiu, J.; Wang, F.; Isoda, S.; Adachi, M. *Chem. Lett.* **2005**, *34*, 1506.
(23) Law, M.; Greene, L. E.; Johnson, J. C.; Saykally, R.; Yang, P. *Nat. Mater.*, **2005**, *4*, 455.
(24) Ohsaki, Y.; Masaki, N.; Kitamura, T.; Wada, Y.; Okamoto, T.; Sekino, T.; Niihara, K.; Yanagida, S. *Phys. Chem. Chem. Phys.* **2005**, *7*, 4157.
(25) Song, M. Y.; Ahn, Y. R.; Jo, S. M.; Kim, D. Y. *Mater. Res. Soc. Symp. Proc.* **2005**, *836*, 107.
(26) Song, M. Y.; Ahn, Y. R.; Jo, S. M.; Kim, D. Y.; Ahn, J.-P. *App. Phys. Lett.* **2005**, *87*, 1713113/1.
(27) Jiu, J.; Isoda, S.; Wang, F.; Adachi, M. *J. Phys. Chem. B* **2006**, *110*, 2087.
(28) Mor, G. K.; Shankar, K.; Paulose, M.; Varghese, O. K.; Grimes, C. A. *Nano Lett.* **2006**, *6*, 215.
(29) Nazeeruddin, M. K.; Splivallo, R.; Liska, P.; Comte, P.; Grätzel, M. *Chem. Commun.* **2003**, *2003*, 1456.
(30) Usami, A. *Chem. Phys. Lett.* **1997**, *277*, 105.
(31) Ferber, J.; Luther, J. *Sol. Energy Mater. Sol. Cells* **1998**, *54*, 265.
(32) Rothenberger, G.; Comte, P.; Gratzel, M. *Sol. Energy Mater. Sol. Cells* **1999**, *58*, 321.
(33) Yoon, J.-H.; Jang, S.-R.; Vittal, R.; Lee, J.; Kim, K.-J. *J. Photochem. Photobiol., A* **2006**, *180*, 184.

(34) Baxter, J. B.; Aydil, E. S. *Sol. Energy Mater. Sol. Cells* **2006**, *90*, 607.

(35) Zaban, A.; Ferrere, S.; Sprague, J.; Gregg, B. A. *J. Phys. Chem. B.* **1997**, *101*, 55

(36) Armstrong, G.; Armstrong, A. R.; Canales, J.; Bruce, P. G. *Chem. Commun.* **2005**, *19*, 2454.

(37) Bandaranayake, K. M. P.; Senevirathna, M. K. I.; Weligamuwa, P. M. G. M. P.; Tennakone, K. *Coord. Chem. Rev.* **2004**, *248*, 1277.

(38) Nakade, S.; Saito, Y.; Kubo, W.; Kitamura, T.; Wada, Y.; Yanagida, S. *J. Phys. Chem. B* **2003**, *107*, 8607.

(39) Grätzel, M. *Pure Appl. Chem.* **2001**, *73*, 459.

(40) Ito, S.; Matsui, H.; Okada, K.-i.; Kusano, S.-i.; Kitamura, T.; Wada, Y.; Yanagida, S. *Sol. Energy Mater. Sol. Cells* **2004**, *82*, 421.

(41) Dürr, M.; Schmid, A.; Obermaier, M.; Rosselli, S.; Yasuda, A.; Nelles, G. *Nat. Mater.* **2005**, *4*, 607.